Polymer Chemistry

ROYAL SOCIETY OF CHEMISTRY

PAPER

View Article Online
View Journal | View Issue

Cite this: *Polym. Chem.*, 2020, **11**, 6953

Rational molecular design of anion exchange membranes functionalized with alicyclic quaternary ammonium cations

Thanh Huong Pham, Andrit Allushi, Joel S. Olsson and Patric Jannasch *

High alkaline stability is critical for polymeric anion exchange membranes (AEMs) and ionomers for use in alkaline electrochemical energy conversion and storage devices such as fuel cells, electrolyzer cells and advanced batteries. Here, we have prepared and studied ether-free polyfluorenes tethered with *N*,*N*-dimethylpiperidinium (DMP) and 6-azonia-spiro[5.5]undecane (ASU) cations, respectively, attached through heteroatom-free alkyl spacers. By employing alkyl–alkyl Suzuki cross-coupling, these alicyclic quaternary ammonium cations are attached at the 4-position to impede ionic loss. Thus, all the β-hydrogens sensitive to elimination reactions are placed in strain-free rings able to fully relax by the spacer flexibility. Consequently, the AEM carrying DMP cations shows a very high alkaline and thermal stability, retaining more than 91% of the cations after 2400 h immersion in 2 M NaOH at 90 °C. Compared with corresponding AEM functionalized with *N*-alkyl-*N*-methylpiperidinium (AMP) cations [conventionally tethered *via* the 1(*N*)-position], the ionic loss by β-elimination is successfully reduced by up to 92%. The AEM functionalized with DMP also reaches a high hydroxide conductivity of 124 mS cm^{-1} at 80 °C. Consequently, tethering piperidine-based cations *via* the 4-position instead of the 1(*N*)-position results in AEMs with substantially improved thermal and alkaline stability, combined with high hydroxide conductivity.

Received 9th September 2020,
Accepted 18th October 2020

DOI: 10.1039/d0py01291b

rsc.li/polymers

1. Introduction

Durable cationic polymers (ionomers) and anion exchange membranes (AEMs) are critical materials for alkaline electrochemical energy technologies such as fuel cells, water electrolyzers, and advanced batteries.[1–8] These devices present a promising alternative to acidic proton exchange membrane applications which require platinum group metal electrocatalysts. Potentially, alkaline devices can operate with lower cost catalysts (*e.g.*, cobalt, silver, and nickel), benefit from faster oxygen reduction and oxygen evolution reactions compared with the acidic environment, and may exploit new electrochemical reactions.[1,9–12] However, the development has been significantly hampered by a lack of AEMs that show high performance in combination with sufficient alkaline stability. Both the backbones and the cations of the polymers in AEMs are susceptible to nucleophilic attack by hydroxide ions. This leads to reduced mechanical strength and losses in ion-exchange capacity (IEC) and conductivity, and hence to irreversible losses in performance and lifetime of the devices.

Polymer backbone degradation in AEMs has primarily been observed to occur *via* aryl ether bonds cleavage,[13–18] motivating a recent change in research focus towards aryl-ether free backbones[19] such as polynorbornenes,[20–24] poly(arylene alkylene)s[25–32] and polystyrenes.[33–38] A more serious issue is the alkaline stability of the tethered cationic groups. These are generally ammonium cations that can degrade by a large number of different mechanisms, including nucleophilic substitutions at α-carbons, elimination of β-hydrogens (Hofmann elimination) and mechanisms unique to the specific structure and configuration of the cation.[1,39–43] In a seminal work, Marino and Kreuer reported on the stability of different model ammonium cations under harsh alkaline conditions (6 M aq. NaOH, 160 °C).[39] The most simple ammonium cation, tetramethylammonium, was found to be very stable with a half-life of $t_{1/2}$ = 62 h, but cannot be tethered to polymers. Tetherable alkyltrimethyl- and tetraalkylammonium cations were much less stable because of the possibility of Hofmann elimination (*e.g.* hexyltrimethyl- and tetrapropylammonium with $t_{1/2}$ = 32 and 7.2 h, respectively).[39] In contrast, the alicyclic piperidine-based *N*,*N*-dimethylpiperidinium (DMP) and 6-azonia-spiro[5.5]undecane (ASU) cations were found to possess an exceptional stability with $t_{1/2}$ = 87 and 110 h, respectively. The reason for their high stability is ascribed to the strain-free rings and the geometric constraint of the rings on the elimin-

Polymer & Materials Chemistry, Department of Chemistry, Lund University, P.O. Box 124, SE-221 00 Lund, Sweden. E-mail: patric.jannasch@chem.lu.se

ation and substitution transition states, which require unfavorable bond angles and lengths.[39] These findings have motivated quite extensive research on AEMs functionalized with piperidine-based cations in recent years.[44–50] However, when these cations are directly incorporated in stiff aromatic polymer backbones, the alkaline stability is significantly reduced in relation to that of the model compounds.[27,28] This has been explained by a distortion of the alicyclic rings by the stiff backbones, which facilitates degradation by Hofmann elimination.[27,28] Hence, in order to benefit from the inherent alkaline stability of the alicyclic cations, these cations must be tethered to the polymer backbone *via* flexible spacer chains that facilitate ring-relaxation and minimize ring-strain.

Another factor that has a significant effect on the alkaline stability of cationic groups in AEMs is the position at which they are attached to the polymer structure.[39] Most studies on AEMs functionalized with piperidinium cations have been carried out on *N*-alkyl-*N*-methylpiperidinium (AMP) tethered to the backbone in the 1(*N*)-position *via* an alkyl chain, (Fig. 1).[49,51,52] This functionalization is readily achieved in Menshutkin reactions of bromoalkylated polymers with *N*-methylpiperidine. Very recently, we have employed this approach to tether AMP to an aryl-ether free polyfluorene (PDPF) backbone.[53] However, this molecular design opens up for Hofmann elimination in the linear alkyl tether. Alternatively, the tethering at the 3- or 4-position instead of the 1(*N*)-position places all the sensitive β-hydrogens in strain-free alicyclic rings, can be expected to significantly reduce Hofmann elimination.

In the present work, we have developed and explored a rational molecular design in which DMP and ASU cations, respectively, are tethered in the 4-positions of the respective rings to PDPF backbones *via* heptyl spacer chains (Scheme 1). Hence, we combine several beneficial molecular design features, including the use of an ether-free backbone and the attachment of piperidine-based cations on flexible spacers which allow full relaxation of the ring strain. The impact of this approach on the thermal and alkaline stability, as well as water uptake and ion conductivity, of the resulting AEMs was subsequently investigated.

2. Results and discussion

2.1. Polymer synthesis

Attaching piperidine-based cations in the 4-position is challenging due to the lack of straightforward synthetic pathways and commercially available building blocks. In the current work this was achieved by attaching 4-methylenepiperidine to a dibromoalkylated diphenylfluorene *via* Suzuki coupling to produce monomer DPF-PiH (Scheme 1). After modification of a published procedure,[54] the synthesis was performed in three steps; hydroboration of *N*-Boc-4-methylene-piperidine with 9-BBN, Suzuki coupling with 9,9-bis(6-bromohexyl)-2,7-diphenyl-9*H*-fluorene (DPF-Br) and finally deprotection in aq. HCl. The key step here is the alkyl–alkyl Suzuki cross-coupling which is a rarely reported reaction, most probably because of the slow oxidative addition of alkyl halides to palladium and facile β-hydride elimination.[54] In order to achieve an efficient Suzuki cross-coupling with DPF-Br, a catalyst system consisting of the bulky and electron-rich phosphine ligand PCy_3, the catalyst $Pd(OAc)_2$ and the base $K_3PO_4{\cdot}H_2O$ was employed. The suc-

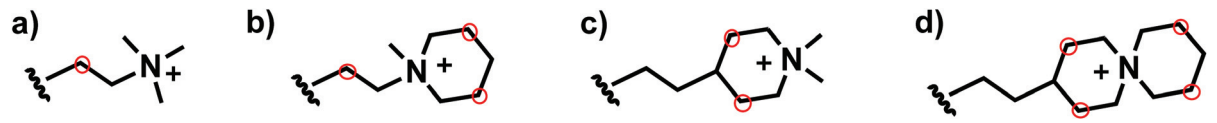

Fig. 1 Cations tethered to polymers *via* alkyl spacers: (a) alkyltrimethylammonium (ATMA), (b) *N*-alkyl-*N*-methylpiperidinium (AMP), (c) 4-alkyl-DMP, and (d) 4-alkyl-ASU. Red circles indicate β-hydrogens with a varied sensitivity towards elimination reactions.

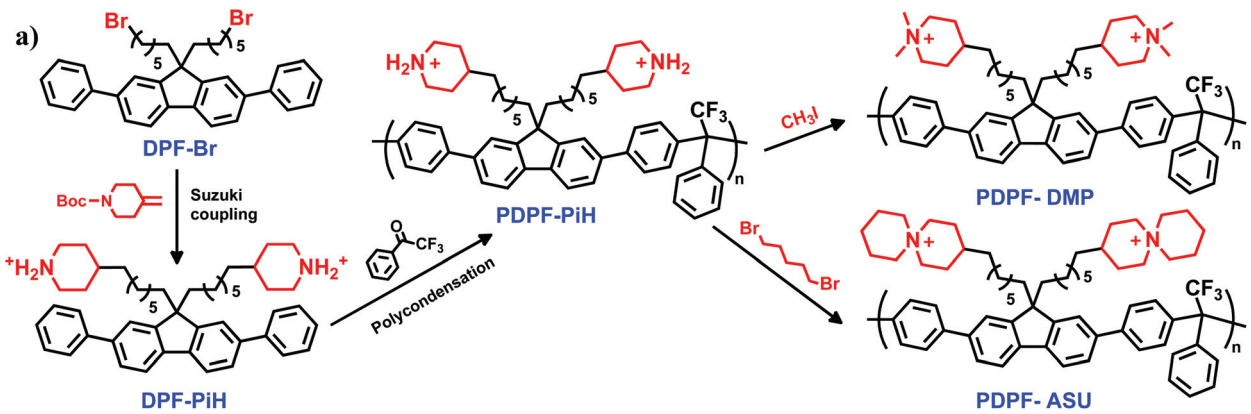

Scheme 1 Synthetic pathway to PDPF-DMP and PDPF-ASU.

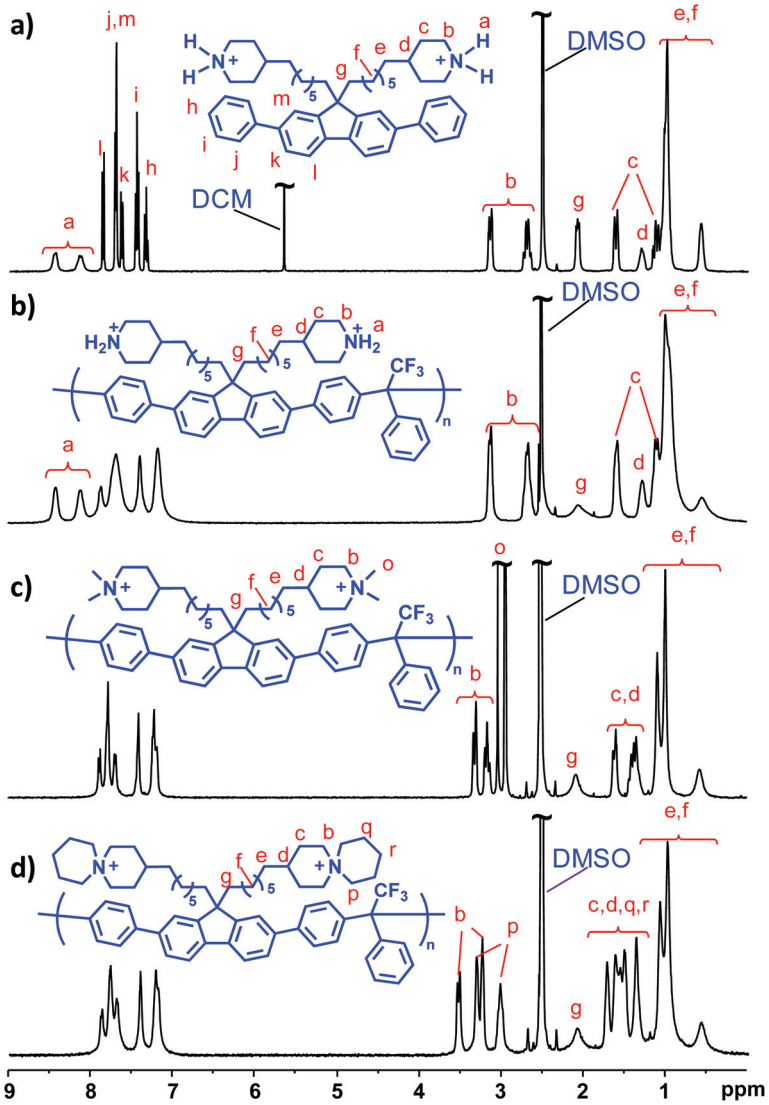

Fig. 2 ^{1}H NMR spectra of (a) DPF-PiH, (b) PDPF-PiH, (c) PDPF-DMP and (d) PDPF-ASU.

cessful synthesis of DPF-PiH was confirmed by ^{1}H NMR spectroscopy (Fig. 2a). As expected, the chemical shifts of the aromatic protons (h–m) and the methylene protons in the alkyl spacers (e, f, g) remained unchanged. Concurrently, the signals originating from the $-CH_2CH_2Br$ and $-CH_2CH_2Br$ protons were replaced by those of the methylene and methine protons of the piperidinium moieties (b, c, d). In addition, the amine protons (a) generated two signals above 8 ppm. Notably, the clear difference in chemical shifts between equatorial and axial protons at *N*-, α- and β-positions (a, b, c) indicated limited conformational change of the ring.

DPF-PiH was subsequently employed in a Friedel–Crafts type polyhydroxyalkylation reaction with 2,2,2-trifluoroacetophenone (TFAp) to produce the precursor homopolymer PDPF-PiH (Scheme 1). Trifluoromethanesulfonic (TFSA) was used as a co-solvent together with dichloromethane to generate the superacidic medium necessary for the polycondensation.[27,55,56] The use of the rather large DPF monomer enables the preparation of well-defined and rigid ether-free PDPF AEMs with the target IEC-range (2.0–2.2 mequiv. g^{-1}) to reach high conductivity without excessive water uptake, thus avoiding the complications of copolymerization. In comparison with for example a backbone based on non-phenylated fluorene, the higher rigidity of the PDPF backbone facilitates film-formation and the mechanical strength of the AEM. Furthermore, DPF-Br is more reactive than the corresponding non-phenylated fluorene monomer in the Friedel–Crafts type polyhydroxyalkylations. In the present case, the high polymerization rate was indicated by the rapid increase in viscosity of the reaction mixture, despite the low temperature (0 °C). After only 1 h, the viscosity became too high for magnetic stirring and the reaction was stopped. The resulting polymer formed transparent and flexible membranes after casting from DMSO solution at 85 °C and the structure of

the polymer was verified by ^{1}H NMR spectroscopy (Fig. 2b). Moreover, PDPF-PiH displayed a high thermal stability and decomposed only above $T_{d,95}$ = 403 °C (5% weight loss) as determined by thermogravimetric analysis (TGA).

Following our previously reported procedures,[27,28,57] the DMP and ASU cations were introduced by quaternizing PDPF-PiH using methyl iodide and 1,5-dibromopentane, respectively, to produce the cationic polymers PDPF-DMP and PDPF-ASU (Scheme 1). In order to avoid potential branching/crosslinking reactions during the cyclo-quaternization in the synthesis of PDPF-ASU, a solution of PDPF-PiH was added drop-wise into a dilute solution of 1,5-dibromopentane. No sign of gelation or particle formation was noted throughout the reaction and the resulting PDPF-ASU had an excellent solubility in DMSO. The formation of both PDPF-DMP and PDPF-ASU from PDPF-PiH was confirmed by NMR spectroscopy. ^{1}H NMR spectra of these samples (Fig. 2c and d) did not show any signal from protonated amine hydrogens (a), hence confirming the complete conversion of the secondary piperidine groups of DPF-PiH. The signals from the piperidinium ring (b, c, d) were shifted downfield, while the signals from the polymer backbone and spacer (e, f, g) remained the same. The two methyl groups in the DMP cation (o) gave rise to two singlets at ~3.04 and 2.93 ppm (Fig. 2c). For the ASU cation, the signals originating from the methylene units of the pendant piperidine ring (p, q, r) appeared at lower chemical shift than the corresponding signals from the piperidine ring attached to the spacer (b, c, d) (Fig. 2d). Due to the restricted conformational change, the shifts of both the α- and β-protons in the pendant rings (p, q) split into two distinct signals in the same manner as the corresponding protons from the piperidine ring attached to the spacer (b, c).

2.2. Membrane characterization

2.2.1 Membrane preparation, water uptake and conductivity. Flexible and transparent AEMs were cast from 5 wt% solutions of PDPF-DMP and PDPF-ASU, respectively, in DMSO at 85 °C (Fig. 3). The IEC determined by Mohr titration of PDPF-DMP (Table 1) was close to the theoretical value, but that of PDPF-ASU was lower than expected. This might be a result of incomplete ion exchange caused by the low water uptake and bulky ASU cations.

Sufficient water uptake is crucial for the formation of a percolating hydrated phase domain, thus directly affects the hydroxide conductivity. After ion-exchange to the hydroxide form, the water uptake of PDPF-ASU and PDPF-DMP at 20 °C was 28 and 58 wt%, respectively (Fig. 4a, Table 1). At 80 °C the values increased to 45 and 111 wt%, respectively (Fig. 4a, Table 1). We have previously observed a significantly lower water uptake of different poly(arylene alkylene)-based AEMs functionalized with ASU cations compared with corresponding membranes carrying DMP cations.[57] In the present case, this observation is probably a combined effect of the lower IEC and the more bulky ASU cations. The swelling (SW) is another important factor that affects the applicability of AEMs. The swelling of both PDPF-ASU and PDPF-DMP in the hydroxide form was seemingly isotropic in water. At room temperature, the in- and through-plane swelling were 8 and 10%, respectively, for PDPF-ASU. For PDPF-DMP, these values were 20 and 22%, respectively. At 80 °C, the in- and through-plane swelling were the same for each AEM and reached 15 and 30% for PDPF-ASU and PDPF-DMP, respectively (Table 1).

As expected, the hydroxide conductivity of the AEMs in the fully hydrated (immersed) state increased with the temperature

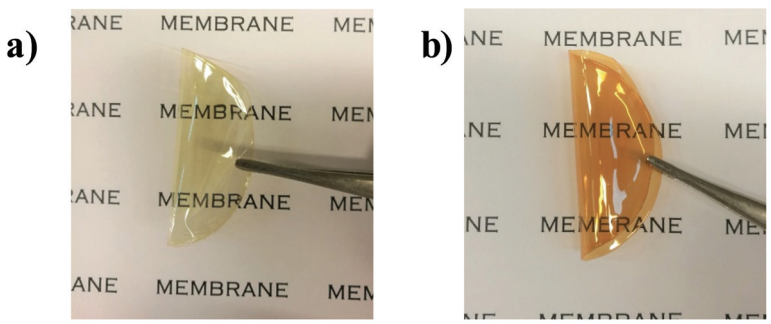

Fig. 3 Photographic images showing folded AEMs cast from (a) PDPF-DMP and (b) PDPF-ASU.

Table 1 Properties of PDPF-DMP and PDPF ASU in comparison with some AEMs reported previously

AEM	IEC_{Br} [mequiv. g^{-1}]		IEC_{OH} [a] [mequiv. g^{-1}]	WU[c] [wt%]	$SW_{in\text{-}plane}$ [c] [%]	$SW_{through\text{-}plane}$ [c] [%]	λ[c]	σ[c] [mS cm^{-1}]	$T_{d,95}$ [d] [°C]
	Theoretical[a]	Titrated[b]							
PDPF-DMP	1.90	1.95 ± 0.03	2.15	111	30	30	29	124	273
PDPF-ASU	1.76	1.62 ± 0.05	1.98	45	15	15	12	76	332

[a] Calculated from the chemical structure of the polymers. [b] Determined by Mohr's titration. [c] Measured at 80 °C in hydroxide form, under fully hydrated conditions (immersed). [d] Measured by TGA under N_2 at 10 °C min^{-1}.

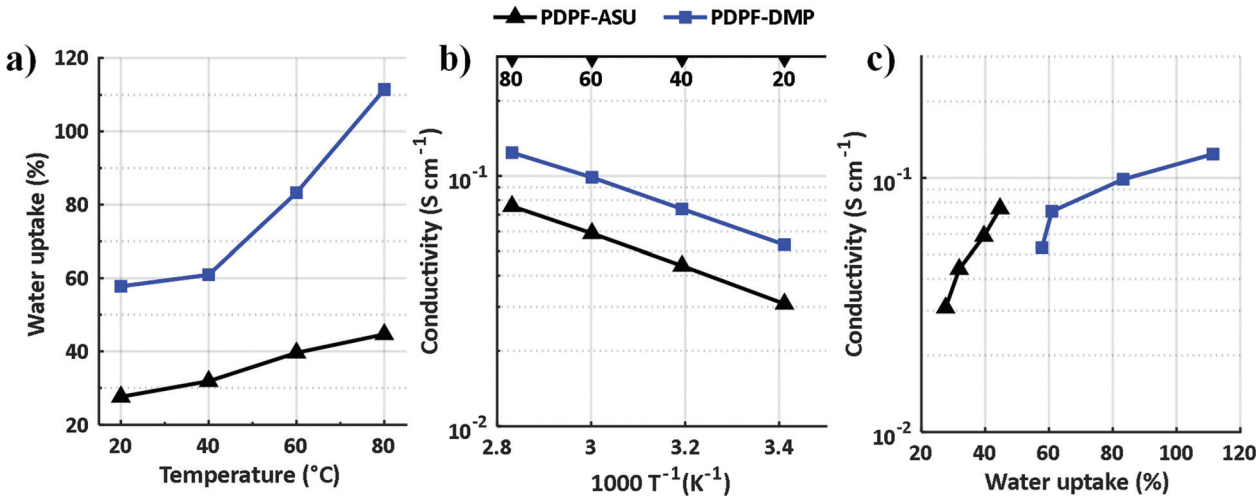

Fig. 4 (a) Water uptake of fully hydrated (immersed) AEMs in the hydroxide form as a function of temperature, (b) hydroxide conductivity of fully hydrated AEMs as a function of T^{-1} and (c) hydroxide conductivity of fully hydrated AEMs as a function of water uptake.

and water uptake (Fig. 4b and c, Table 1). At 20 and 80 °C, PDPF-ASU showed a conductivity (σ) of 31 and 76 mS cm^{-1}, respectively. PDPF-DMP reached a very high conductivity, 53 and 124 mS cm^{-1} under the same conditions. Hence, the conductivity of PDPF-DMP was significantly higher than PDPF-ASU at 80 °C. The conductivity results are in good agreement with previous findings on AEMs with DMP and ASU cations directly attached to the poly(arylene alkylene)s.[57] Beside the higher IEC and water uptake, the less bulky DMP cations might also facilitate ion clustering during casting, thus promoting phase separation and ion transport. The conductivity of PDPF-DMP was comparable or significantly higher than with that of AEMs with similar or higher IEC (Table 2),[46–48,53,58] demonstrating the advantages of the present molecular design on the hydroxide conductivity of AEMs.

2.2.2 Thermal and chemical stability. The main focus of the present work was to identify pathways towards improved thermal and chemical stability of AEMs by rational design of alicyclic cations tethered to ether-free polymers *via* alkyl spacers. Thermogravimetrical measurements showed that AEMs based on PDPF-DMP and PDPF-ASU decomposed at $T_{d,95}$ = 273 and 332 °C, respectively, (Fig. 5). Most probably, the higher rigidity of the ASU cation in comparison with the monocyclic DMP was the reason for the significantly higher decomposition temperature of the latter. By comparing with our previous work, the attachment position of the piperidinium rings had a significant effect on the thermal stability. By attachment in the 4-instead of the 1(*N*)-position, the formation of the more unstable AMP cation was avoided. Consequently, the $T_{d,95}$ value of PDPF-DMP (Fig. 6) was ~70 °C higher than that of PDPF-Pip, the corresponding AEM functionalized with AMP instead of DMP.[53] In contrast, the effect of the alkyl spacer length was seemingly less important as the $T_{d,95}$ values are similar to corresponding poly(arylene alkylene)-based AEMs with DMP and ASU cations attached directly to the polymer backbone[27,28] or *via* short alkyl spacers.[57]

In order to investigate the alkaline stability, the AEMs were immersed in 2, 5, 7 and 10 M aq. NaOH solutions at 90 °C for different periods of time, followed by ^{1}H NMR analysis of any

Table 2 Properties of PDPF-DMP and PDPF-ASU in comparison with previously reported AEMs

				Structure				
AEM	IEC[a] [mequiv. g^{-1}]	WU[b] [wt%]	σ[b] [mS cm^{-1}]	Backbone	Cation	Spacer	Attachment position	Ref.
PDPF-DMP	2.15	111	124	PDPF-based	DMP	Alkyl	4	Present
PDPF-ASU	1.98	45	76	PDPF-based	ASU	Alkyl	4	Present
PDPF-TMA	2.24	178	107	PDPF-based	ATMA	Alkyl	1(*N*)	53
PFF$^+$	2.45	26	48	Fluorene-based	ATMA	Alkyl	1(*N*)	58
PBF2	2.19	160	86	Fluorene-based	AMP	Alkyl	1(*N*)	47
PBPipQ66Ap	2.24	141	118	Biphenyl-based	DMP	None	4	59
QPES	1.89	20–25	59.8	Polysulfone	DMP	None	4	48
PPO-DMP	1.98[c]	—	71.8	Poly(phenylene oxide)	DMP	Triazolium	4	46

[a] Calculated from the chemical structure of the polymers in hydroxide form. [b] Measured at 80 °C in hydroxide form under fully hydrated conditions (immersed). [c] Determined by acid–base titration.

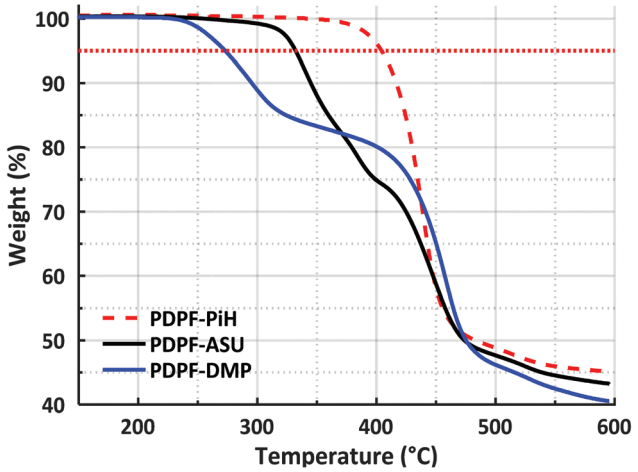

Fig. 5 TGA profiles of PDPF-PiH, PDPF-ASU and PDPF-DMP (dotted horizontal line indicates the 95 wt% limit).

changes in molecular structure. These alkali concentrations correspond to λ ($[H_2O]/[OH^-]$) values of approximately 10.6, 7.4 and 5.0, respectively. All AEM samples remained transparent and were seemingly unaffected after the alkaline stability study. In addition, there was no detectable change in the aromatic region of the NMR spectra, confirming the high stability of the ether-free polymer backbone. In contrast, signs of cationic degradation was indicated by the appearance of new small signals outside the aromatic region (Fig. 6 and 7a). The alicyclic DMP and ASU cations degrade mainly *via* nucleophilic substitution and Hofmann elimination.[39] Both degradation pathways lead to formation of tertiary amines, which were protonated upon addition of TFA and gave rise to NMR signals above 8 ppm (Fig. 6 and 7a). By comparing the intensity of these signals with that of the stable aromatic signals, the total ionic loss was estimated. Concurrently, degradation *via* Hofmann elimination resulted in the formation of alkene groups, which were readily detected by the appearance of dis-

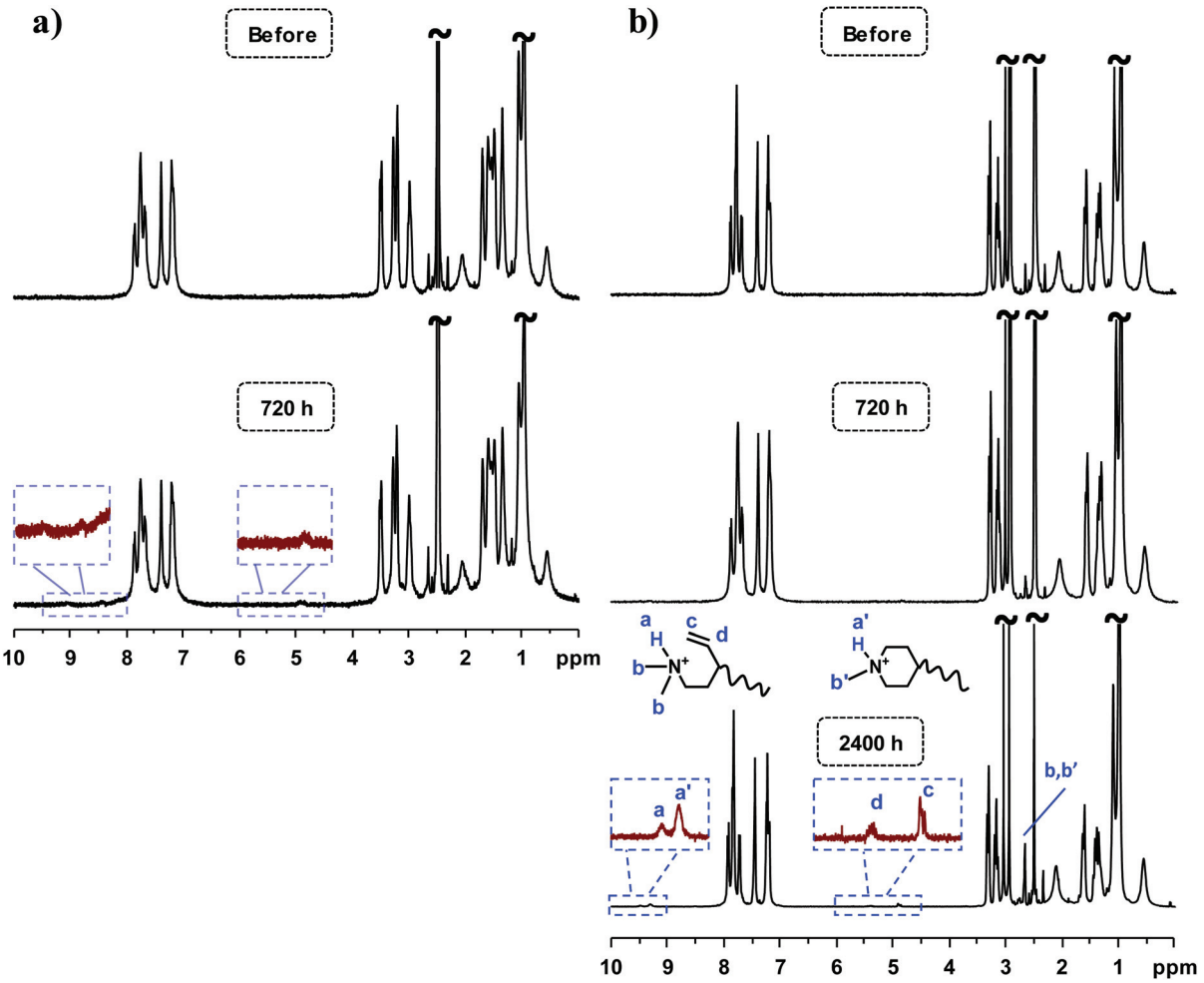

Fig. 6 ^{1}H-NMR spectra of (a) PDPF-ASU and (b) PDPF-DMP before and after immersion in 2 M aq. NaOH solutions at 90 °C. TFA was added to shift the water signals (originally at ~3.3 ppm) to above 10 ppm, revealing sample signals between 3.0 and 3.5 ppm (no data available for PDPF-ASU after 2400 h because of insolubility).

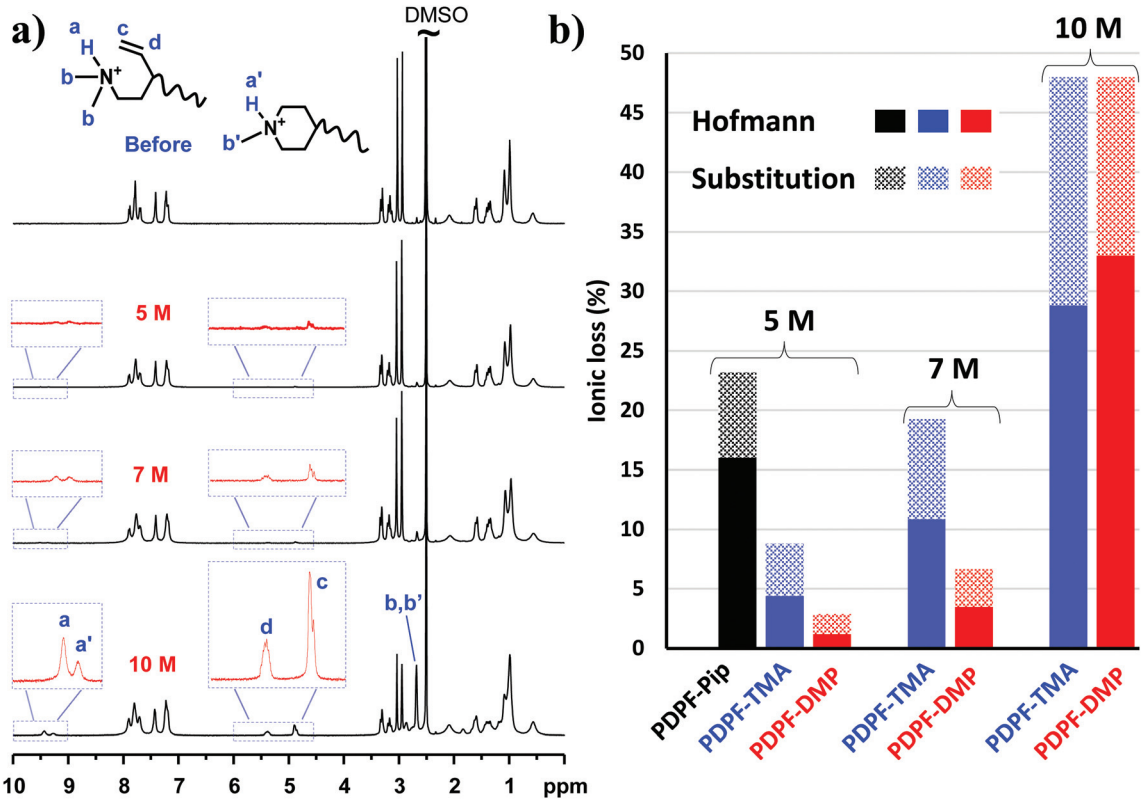

Fig. 7 Alkaline stability of AEMs immersed in 5, 7 and 10 M aq. NaOH solutions during 168 h: (a) ^{1}H NMR spectra of PDPF-DMP before and after immersion (TFA was added to shift the water signals originally at ~3.3 ppm to above 10 ppm, revealing sample signals between 3.0 and 3.5 ppm) and (b) the ionic loss of PDPF-Pip, PDPF-TMA and PDPF-DMP *via* Hofmann elimination and substitution reactions, respectively.

tinct vinyl signals between 4.5 and 5.5 ppm. Integration of these signals gave the quantitative ionic loss caused by Hofmann elimination exclusively.

PDPF-ASU showed traces of degradation already after 720 h immersion in 2 M aq. NaOH (Fig. 6a), and the solubility of PDPF-ASU was found to decrease after further alkaline treatment. The solubility decreased both with the treatment time and the alkali concentration which prevented further studies of the alkaline stability of this AEM. The decrease in solubility was most probably due to crosslinking *via* the degradation products, *e.g.*, through amino alcoholates formed in the ring-opening substitution of ASU. The alcoholates may then react with ASU rings *via* nucleophilic attack, resulting in ether-containing crosslinks.

PDPF-DMP had a higher alkaline stability compared to PDPF-ASU. After 720 h immersion of PDPF-DMP in aq. NaOH solution at 90 °C, no detectable change was observed in the ^{1}H NMR spectra, suggesting excellent alkaline stability (Fig. 6b). In contrast to PDPF-ASU, PDPF-DMP remained completely soluble in DMSO after the alkaline treatment, suggesting different degradation mechanisms for the two cations. After 2400 h immersion in 2 M aq. NaOH, the total ionic loss of PDPF-DMP remained very low at 8.4%, of which a mere 2.0% was attributed to β-elimination (Fig. 6b, Table 3).

Table 3 Ionic loss after alkaline treatment of PDPF-DMP at 90 °C, as evaluated from ^{1}H NMR data

	Ionic loss [%]		
Treatment	Hofmann elimination	Nucleophilic substitution	Total
2 M NaOH, 2400 h	2.0	6.4	8.4
5 M NaOH, 168 h	1.2	1.7	2.9
7 M NaOH, 168 h	3.5	3.2	6.7
10 M NaOH, 168 h	33	15	48

As expected, the rate of degradation increased with the concentration of alkali. Consequently, PDPF-DMP showed signs of degradation after 168 h immersion in 5, 7 and 10 M aq. NaOH solutions at 90 °C (Fig. 7a). Notably, the relative rates of the different degradation pathways varied with the alkaline concentration. With increasing NaOH concentration, the rate of Hofmann elimination accelerated much faster than nucleophilic substitution (Fig. 7b, Table 3). At 10 M, Hofmann elimination became the dominating degradation pathway instead of nucleophilic substitution that dominated at 2 M. Moreover, while PDPF-DMP remained quite stable in 5 M and 7 M aq. NaOH (<10% ionic loss), an increase of alkaline concentration

from 7 to 10 M resulted in a sharp increase in the total ionic loss, probably due to increased reactivity of the OH^- at this very low λ-value (Fig. 7b, Table 3).[60]

The positive effect on the alkaline stability by attaching *via* the 4-position is apparent when comparing the alkaline stability of PDPF-DMP with corresponding AEMs functionalized with AMP (designated PDPF-Pip) and ATMA (designated PDPF-TMA, cations attached at 1(*N*)-position, Fig. 1).[53] The alkaline stability of the two latter AEMs have previously been investigated under conditions similar to those used in the present study (Fig. 7b). After 168 h immersion in 5 M aq. NaOH, the total ionic loss in PDPF-DMP was merely 2.9% (Table 3), nearly 5-fold less than the ionic loss in PDPF-Pip.[53] While the loss *via* nucleophilic substitution was similar for both cations, the Hofmann elimination of the former was reduced by 92%. Furthermore, PDPF-DMP also showed higher alkaline stability than the corresponding AEM functionalized with the benchmark ATMA cation (PDPF-TMA).[53] While both polymers showed a similar total ionic loss in 10 M aq. NaOH, PDPF-DMP had ~3 times less ionic loss than the latter in 5 and 7 M aq. NaOH solutions (Fig. 7b).

3. Conclusions

We have successfully employed alkyl–alkyl Suzuki cross-coupling to attach piperidine-based DMP and ASU cations at the 4-position to ether-free polyfluorenes *via* alkyl spacers. This approach allowed a molecular design in which all the sensitive β-hydrogens were placed in strain-free alicyclic rings able to fully relax by the flexibility of the spacers. Compared with AEMs conventionally tethered with AMP cations *via* the 1(*N*)-position, corresponding AEMs with DMP cations attached *via* the 4-position showed significantly improved thermal and alkaline stability, while retaining high hydroxide conductivity. After immersion in concentrated (5 M) alkali at 90 °C, the total ionic loss was 80% lower for DMP compared with AMP. While the loss by substitution was approximately the same for both cations, the loss by β-elimination was an order of magnitude lower for DMP compared to AMP. Concurrently, the total ionic loss of DMP was 67% lower than of ATMA. However, in highly concentrated alkali (10 M), the ionic loss of DMP was in the same range as that of ATMA. The findings of the study demonstrate that AEMs with high hydroxide conductivity and substantially improved thermal and alkaline stability are obtained by employing a molecular design where piperidine-based cations are tethered to ether-free aromatic polymers *via* the 4-position instead of the 1(*N*)-position.

4. Experimental

1-*N*-Boc-4-methylene-piperidine (96%, Fluorochem), 9-borabicyclo[3.3.1]nonane (9BBN, 0.5 M in THF, Sigma-Aldrich), potassium phosphate (K_3PO_4, ≥99%, Sigma-Aldrich tetrakis(triphenylphosphine)palladium(0) (99%, Sigma-Aldrich), tricyclohexylphosphine (PCy3, reagent grade, Sigma-Aldrich), HCl (37% in water, VWR), 2,2,2-trifluoroacetophenone (TFAp, 99%, Sigma-Aldrich), 1,1,1-trifluoroacetic acid (TFA, 99%, Acros), triflic acid (TFSA, 99%, Acros), 1,5-dibromopentane (97%, Aldrich), *N*,*N*-diisopropylethylamine (DIPEA, ≥99%, Sigma-Aldrich), methyliodide (99%, Sigma-Aldrich), K_2CO_3 (99%, Sigma-Aldrich), toluene (reagent grade, VWR), isopropanol (IPA, reagent grade, VWR), diethyl ether (Et_2O, reagent grade, VWR), *N*-methyl-2-pyrrolidone (NMP, reagent grade, Acros), dimethyl sulfoxide (DMSO, reagent grade, VWR), ethyl acetate (EtOAc, reagent grade, VWR), heptane (reagent grade, VWR), NaBr (99%, Sigma-Aldrich), ethanol (EtOH, 99.5%, Solveco), NaOH (99% pellets, VWR), KOH (99% pellets, VWR), $CDCl_3$ (99.8 atom% D, Sigma-Aldrich) and DMSO-d_6 (99.5 atom% D, Sigma-Aldrich) were all used as received. Dichloromethane was dried using an MBraun dry solvent dispenser system MB-SPS 800. 2,7-Diphenyl-9,9-bis(6-bromohexyl)-fluorene (DPF-Br) was synthesized following a previously published procedure.[53]

4.1. Monomer and polymer synthesis

4.1.1 4,4′-((2,7-Diphenyl-9*H*-fluorene-9,9-diyl) bis(heptane-7,1-diyl))dipiperidine (DPF-PiH). The synthesis of DPF-PiH was done under argon atmosphere. 1-*N*-Boc-4-methylene-piperidine (2.23 g, 11.3 mmol, 2.4 eq.) was added in a 50 ml one-neck round flask, then degassed and cooled to 0 °C using an ice bath. Solution of 0.5 M 9BBN in THF (22.6 ml, 11.3 mmol, 2.4 eq.) was added and the reaction mixture was stirred for 2 h before the ice bath was removed. The reaction mixture was stirred at RT for additional 2 h, then degassed and added into a degassed mixture of DPF-Br (3.04 g, 4.72 mmol, 1 eq.), K_3PO_4 (2.40 g, 11.3 mmol, 2.4 eq.), $Pd(OAc)_2$ (0.169 g, 0.755 mmol, 0.16 eq.), THF (12 ml) and DI water (0.2 ml) in a 100 ml two-neck round flask equipped with condenser and argon inlet. The mixture was stirred at 60 °C for 3 days. After cooled to RT, the reaction mixture was quickly passed through a silica plug. The plug was rinsed thoroughly with diethyl ether and the combined filtrate was evaporated until dryness under reduced pressure. The crude product was then purified further by dry column vacuum chromatography,[61] using gradient EtOAc : heptane mixtures (0 : 100 to 30 : 70) as eluent to yield a viscous oil. The oil was then stirred with concentrated aq. HCl (7 ml) in a 25 ml round flask overnight. The mixture was evaporated until dryness under reduced pressure and the residue was stirred vigorously in acetone at 0 °C, then filtrated to yield DPF-PiH as a white powder.

4.1.2 Precursor polymer PDPF-PiH. TFSA (2.7 ml, 30 mmol, 11 eq.) was added dropwise to a mixture of DPF-PiH (2.075 g, 2.76 mmol, 1 eq.), TFAp (0.426 ml, 3.036 mmol, 1.1 eq.) and anhydrous DCM (2.7 ml) in a 25 ml round flask at 0 °C under N_2 atmosphere and the mixture was stirred with a magnetic stirrer. After 1 h, the highly viscous mixture was poured into cold DI water. The polymer precipitation was crushed using a mortar and pestle and washed repeatedly with DI water. The obtained polymer (PDPF-PiH) was subsequently dried under

vacuum at RT, then dissolved in DMSO to give ~10 wt% solution. This solution was cast at 80 °C, giving a transparent membrane of PDPF-PiH. The membrane was then washed with IPA and water, and dried under vacuum at RT.

4.1.3 Membrane polymer PDPF-DMP. Polymer PDPF-PiH (0.7 g, 0.615 mmol, 1 eq.), K_2CO_3 (0.51 g, 3.69 mmol, 6 eq.), NMP (3.5 ml), DMSO (3.5 ml) and MeI (0.31 ml, 4.9 mmol, 8 eq.) was added in a 25 ml one-neck round bottom flask. The bottle was then covered in aluminium foil to prevent degradation of MeI and the mixture was stirred at RT for 48 h. The product was then precipitated in ~0.1 M aq. NaBr solution, washed repeatedly in NaBr solution and water and dried under vacuum to give PDPF-PiH as a light yellow powder.

4.1.4 Membrane polymer PDPF-ASU. A solution of polymer PDPF-PiH (0.6 g, 0.528 mmol, 1 eq.) in DMSO (12 ml) was added dropwise into a 50 ml round bottom flask containing 1,5-dibromopentane (0.158 ml, 1.16 mmol, 2.2 eq.), DIPEA (0.92 ml, 5.3 mmol, 10 eq.) and NMP (12 ml) at 80 °C. The reaction mixture was stirred at 80 °C for 72 h. The product was then precipitated in a mixture of diethyl ether and IPA, washed repeatedly with diethyl ether and water and dried under vacuum to give PDPF-ASU as an orange powder.

4.1.5 Membrane preparation. The AEMs were cast from 5% polymer solutions in DMSO at 85 °C. Approximately 0.15 g polymer was dissolved in DMSO to obtain 3 g solution. This solution was filtrated through a syringe-driven filter unit (∅ = 25 mm, Fluoropore membrane, 5 μm) into a Petri dish (∅ = 50 mm) which was then placed in a ventilated casting oven at 80 °C for at least 24 h. Afterward, the resulting AEM was immersed in 1 M aq. NaBr solution for at least 7 days to exchange all the counter ions to bromide, then washed thoroughly with DI water and stored in DI water.

The AEM in the in hydroxide form was prepared from bromide form by ion-exchange in 1 M aq. NaOH solution at RT for at least 120 h. After that the membrane was washed thoroughly with degassed deionized water and stored (if necessary) in degassed deionized water under nitrogen for less than 72 h before the measurement.

4.2. Characterization

4.2.1 NMR spectroscopy. The molecular structure of the polymers was confirmed by ^{1}H NMR spectra recorded at 400 MHz, using a Bruker DRX 400 spectrometer. The solvent used was a mixture of DMSO-d_6 and TFA.

4.2.2 Intrinsic viscosity. The intrinsic viscosity of the precursor polymers PDPF-PiH was measured at 30 °C using an Ubbelohde viscometer. The sample was dried at 50 °C under vacuum for at least 48 h, weighed, and dissolved in 0.1 M LiBr in DMSO solution (blank solution) to obtain a stock solution with concentration 0.992 g dL^{-1}. The solution was later diluted with the blank solution to obtain three solutions with concentration 0.873, 0.704 and 0.532 g dL^{-1}. The resulting solutions were used immediately after preparation. The flow times through the capillary of the blank solution (t_{blank}) and of the polymer solutions (t_{sample}) were taken as the average of four measurements. The inherent (η_{inh}) and reduced (η_{red}) viscosities at four different concentrations were calculated as:[42]

$$\eta_{inh} = \frac{\ln\left(\frac{t_{sample}}{t_{blank}}\right)}{C} \quad (1)$$

$$\eta_{red} = \frac{\frac{t_{sample}}{t_{blank}} - 1}{C}. \quad (2)$$

The intrinsic viscosity ($[\eta]$) was calculated to be 0.19 dL g^{-1} by taking the average of the intersections of the linear regressions of η_{inh} and η_{red} with the y-axis.

4.2.3 Thermal decomposition. The thermal decomposition of the AEMs PDPF-DMP and PDPF-ASU in the bromide form and of precursor polymer PDPF-PiH in the protonated state with triflate counter ions was studied by thermogravimetric analysis (TGA) using a TGA Q500 (TA Instruments) during heating from 50 to 600 °C at 10 °C min^{-1} under N_2 atmosphere. In order to remove water residues, the samples were kept isothermally at 120 °C for 20 min prior to the analysis. The thermal decomposition temperature was reported at 5% weight loss ($T_{d,95}$).

4.2.4 Ion exchange capacity. The IEC of the AEMs in the bromide (IEC_{Br}) form was determined by titration. The membranes were first dried at 50 °C under vacuum during 48 h and weighed to obtain their dry weights. The dry membranes were then immersed in 25 ml 0.2 M aq. $NaNO_3$ solution at 40–50 °C for 7 days. The solutions were titrated with an aq. $AgNO_3$ solution (approx. 0.01 M), using an aq. K_2CrO_4 solution (0.1 M) as the indicator. The IEC of the AEMs in the hydroxide form (IEC_{OH}) was calculated from the IEC_{Br} as

$$IEC_{OH} = \frac{IEC_{Br}}{1 - 0.0629 \times IEC_{Br}}. \quad (3)$$

4.2.5 Water uptake and swelling ratio. The dry weight, length and thickness of the membranes ($m_{dry,Br}$, l_{dry}, t_{dry}) in bromide form was measured after 48 h drying at 50 °C under vacuum. By assuming that all Br^- was exchanged to OH^-, the dry weight of the AEMs in the hydroxide form (m_{dry}) was calculated from $m_{dry,Br}$ as:

$$m_{dry} = m_{dry,Br} \times (1 - 0.0629 \times IEC_{BR}). \quad (4)$$

Afterward, the AEMs were ion-exchanged to hydroxide form. The weight, length and thickness of the hydrated membranes (m_{wet}, l_{wet}, t_{wet}) were obtained after equilibration in DI water at 20, 40, 60 and 80 °C. Their water uptake was calculated as:

$$WU = \frac{m_{wet} - m_{dry}}{m_{dry}} \times 100\,(\%). \quad (5)$$

The membrane swelling, *i.e.*, the increase in length and thickness of the membranes, was calculated in similar way to the water uptake. Hence, the in-plane swelling was the average increase in length of the four edges of the quadrangular membranes, and the through-plane swelling was the average increase in thickness at the four corners.

4.2.6 Hydroxide conductivity. The hydroxide ion conductivity of the hydrated AEMs was measured by electrochemical impedance spectroscopy using a two-probe set-up and a Novocontrol high-resolution dielectric analyzer V 1.01S. During the measurements, these membranes were kept hydrated in a closed cell filled with deionised degassed water. The voltage amplitude was kept at 50 mV while varying the frequency from 10^7 to 10^0 Hz in the temperature range of 20 to 80 °C.

4.2.7 Alkaline stability. The alkaline stability of all AEMs in 2 M, 5 M, 7 M and 10 M aq. NaOH at 90 °C was evaluated after immersion in respective solutions for different periods of time. After the immersion, these membranes were exchanged to the bromide form by immersion in aq. 1 M NaBr solution overnight. The membranes were then dried and dissolved in mixtures of DMSO-d_6 and TFA, and analyzed by ^{1}H NMR spectroscopy.

Conflicts of interest

There are no conflicts to declare.

Acknowledgements

We thank the Swedish Energy Agency (grants 45057-1 and 37806-3), the Swedish Research Council (grants 45397-1 and 2015-04820) and the Swedish Foundation for Strategic Research, SSF, (grant EM16-0060) for financial support.

References

1 J. R. Varcoe, P. Atanassov, D. R. Dekel, A. M. Herring, M. A. Hickner, P. A. Kohl, A. R. Kucernak, W. E. Mustain, K. Nijmeijer, K. Scott, T. Xu and L. Zhuang, *Energy Environ. Sci.*, 2014, **7**, 3135–3191.
2 M. A. Hickner, A. M. Herring and E. B. Coughlin, *J. Polym. Sci., Part B: Polym. Phys.*, 2013, **51**, 1727–1735.
3 D. R. Dekel, *J. Power Sources*, 2018, **375**, 158–169.
4 S. Gottesfeld, D. R. Dekel, M. Page, C. Bae, Y. Yan, P. Zelenay and Y. S. Kim, *J. Power Sources*, 2018, **375**, 170–184.
5 C. G. Arges and L. Zhang, *ACS Appl. Energy Mater.*, 2018, **1**, 2991–3012.
6 B. Dunn, H. Kamath and J.-M. Tarascon, *Science*, 2011, **334**, 928–935.
7 Z. P. Cano, D. Banham, S. Ye, A. Hintennach, J. Lu, M. Fowler and Z. Chen, *Nat. Energy*, 2018, **3**, 279–289.
8 K. Zeng and D. Zhang, *Prog. Energy Combust. Sci.*, 2010, **36**, 307–326.
9 S. D. Poynton, J. P. Kizewski, R. C. T. Slade and J. R. Varcoe, *Solid State Ionics*, 2010, **181**, 219–222.
10 S. Gu, W. Sheng, R. Cai, S. M. Alia, S. Song, K. O. Jensen and Y. Yan, *Chem. Commun.*, 2013, **49**, 131–133.
11 T. S. Olson, S. Pylypenko, P. Atanassov, K. Asazawa, K. Yamada and H. Tanaka, *J. Phys. Chem. C*, 2010, **114**, 5049–5059.
12 G. Merle, M. Wessling and K. Nijmeijer, *J. Membr. Sci.*, 2011, **377**, 1–35.
13 S. Miyanishi and T. Yamaguchi, *Phys. Chem. Chem. Phys.*, 2016, **18**, 12009–12023.
14 C. Fujimoto, D.-S. Kim, M. Hibbs, D. Wrobleski and Y. S. Kim, *J. Membr. Sci.*, 2012, **423–424**, 438–449.
15 Y.-K. Choe, C. Fujimoto, K.-S. Lee, L. T. Dalton, K. Ayers, N. J. Henson and Y. S. Kim, *Chem. Mater.*, 2014, **26**, 5675–5682.
16 C. G. Arges and V. Ramani, *Proc. Natl. Acad. Sci. U. S. A.*, 2013, **110**, 2490–2495.
17 A. D. Mohanty, S. E. Tignor, J. A. Krause, Y. K. Choe and C. Bae, *Macromolecules*, 2016, **49**, 3361–3372.
18 A. Amel, L. Zhu, M. Hickner and Y. Ein-Eli, *J. Electrochem. Soc.*, 2014, **161**, F615–F621.
19 S. Noh, J. Y. Jeon, S. Adhikari, Y. S. Kim and C. Bae, *Acc. Chem. Res.*, 2019, **52**, 2745–2755.
20 C. Wang, B. Mo, Z. He, Q. Shao, D. Pan, E. Wujick, J. Guo, X. Xie, X. Xie and Z. Guo, *J. Membr. Sci.*, 2018, **556**, 118–125.
21 C. Wang, B. Mo, Z. He, X. Xie, C. X. Zhao, L. Zhang, Q. Shao, X. Guo, E. K. Wujcik and Z. Guo, *Polymer*, 2018, **138**, 363–368.
22 W. Chen, M. Mandal, G. Huang, X. Wu, G. He and P. A. Kohl, *ACS Appl. Energy Mater.*, 2019, **2**, 2458–2468.
23 G. Huang, M. Mandal, X. Peng, A. C. Yang-Neyerlin, B. S. Pivovar, W. E. Mustain and P. A. Kohl, *J. Electrochem. Soc.*, 2019, **166**, F637–F644.
24 M. Mandal, G. Huang and P. A. Kohl, *J. Membr. Sci.*, 2019, **570–571**, 394–402.
25 W.-H. Lee, Y. S. Kim and C. Bae, *ACS Macro Lett.*, 2015, **4**, 814–818.
26 W.-H. Lee, E. J. Park, J. Han, D. W. Shin, Y. S. Kim and C. Bae, *ACS Macro Lett.*, 2017, **6**, 566–570.
27 J. S. Olsson, T. H. Pham and P. Jannasch, *Adv. Funct. Mater.*, 2018, **28**, 1702758.
28 T. H. Pham, J. S. Olsson and P. Jannasch, *J. Mater. Chem. A*, 2018, **6**, 16537–16547.
29 M. Ozawa, T. Kimura, K. Otsuji, R. Akiyama, J. Miyake, M. Uchida, J. Inukai and K. Miyatake, *ACS Omega*, 2018, **3**, 16143–16149.
30 S. Maurya, S. Noh, I. Matanovic, E. J. Park, C. N. Villarrubia, U. Martinez, J. Han, C. Bae and Y. S. Kim, *Energy Environ. Sci.*, 2018, **11**, 3283–3291.
31 H. Ono, T. Kimura, A. Takano, K. Asazawa, J. Miyake, J. Inukai and K. Miyatake, *J. Mater. Chem. A*, 2017, **5**, 24804–24812.
32 A. M. A. Mahmoud and K. Miyatake, *J. Mater. Chem. A*, 2018, **6**, 14400–14409.
33 A. D. Mohanty, C. Y. Ryu, Y. S. Kim and C. Bae, *Macromolecules*, 2015, **48**, 7085–7095.
34 S. K. Tuli, A. L. Roy, R. A. Elgammal, T. A. Zawodzinski and T. Fujiwara, *Polym. Int.*, 2018, **67**, 1302–1312.

35 J. Ponce-González, D. K. Whelligan, L. Wang, R. Bance-Soualhi, Y. Wang, Y. Peng, H. Peng, D. C. Apperley, H. N. Sarode, T. P. Pandey, A. G. Divekar, S. Seifert, A. M. Herring, L. Zhuang and J. R. Varcoe, *Energy Environ. Sci.*, 2016, **9**, 3724–3735.
36 J. Hao, X. Gao, Y. Jiang, H. Zhang, J. Luo, Z. Shao and B. Yi, *J. Membr. Sci.*, 2018, **551**, 66–75.
37 Z. Wang, J. Parrondo and V. Ramani, *J. Electrochem. Soc.*, 2017, **164**, F1216–F1225.
38 J. S. Olsson, T. H. Pham and P. Jannasch, *Macromolecules*, 2020, **53**, 4722–4732.
39 M. G. Marino and K. D. Kreuer, *ChemSusChem*, 2015, **8**, 513–523.
40 J. B. Edson, C. S. Macomber, B. S. Pivovar and J. M. Boncella, *J. Membr. Sci.*, 2012, **399–400**, 49–59.
41 S. Chempath, B. R. Einsla, L. R. Pratt, C. S. Macomber, J. M. Boncella, J. A. Rau and B. S. Pivovar, *J. Phys. Chem. C*, 2008, **112**, 3179–3182.
42 G. Cerichelli, G. Illuminati and C. Lillocci, *J. Org. Chem.*, 1980, **45**, 3952–3957.
43 A. C. Cope and A. S. Mehta, *J. Am. Chem. Soc.*, 1963, **85**, 1949–1952.
44 N. Chen, C. Long, Y. Li, C. Lu and H. Zhu, *ACS Appl. Mater. Interfaces*, 2018, **10**, 15720–15732.
45 X. Chu, L. Liu, Y. Huang, M. D. Guiver and N. Li, *J. Membr. Sci.*, 2019, **578**, 239–250.
46 H. J. Park, X. Chu, S. P. Kim, D. Choi, J. W. Jung, J. Woo, S. Y. Baek, S. J. Yoo, Y.-C. Chung, J. G. Seong, S. Y. Lee, N. Li and Y. M. Lee, *J. Membr. Sci.*, 2020, **608**, 118183.
47 R. Ren, S. Zhang, H. A. Miller, F. Vizza, J. R. Varcoe and Q. He, *ACS Appl. Energy Mater.*, 2019, **2**, 4576–4581.
48 F. Wang, B. Xue, S. Zhou, J. Zheng, S. Li, S. Zhang and T. A. Sherazi, *J. Membr. Sci.*, 2019, **591**, 117334.
49 X. Chu, Y. Shi, L. Liu, Y. Huang and N. Li, *J. Mater. Chem. A*, 2019, **7**, 7717–7727.
50 J. Wang, Y. Zhao, B. P. Setzler, S. Rojas-Carbonell, C. B. Yehuda, A. Amel, M. Page, L. Wang, K. Hu, L. Shi, S. Gottesfeld, B. Xu and Y. Yan, *Nat. Energy*, 2019, **4**, 392–398.
51 H.-S. Dang and P. Jannasch, *J. Mater. Chem. A*, 2016, **4**, 11924–11938.
52 M. Niu, C. Zhang, G. He, F. Zhang and X. Wu, *Int. J. Hydrogen Energy*, 2019, **44**, 15482–15493.
53 A. Allushi, T. H. Pham, J. S. Olsson and P. Jannasch, *J. Mater. Chem. A*, 2019, **7**, 27164–27174.
54 M. R. Netherton, C. Dai, K. Neuschütz and G. C. Fu, *J. Am. Chem. Soc.*, 2001, **123**, 10099–10100.
55 D. A. Klumpp, M. Garza, A. Jones and S. Mendoza, *J. Org. Chem.*, 1999, **64**, 6702–6705.
56 M. J. O'Connor, K. N. Boblak, A. D. Spitzer, P. A. Gucciardo, A. M. Baumann, J. W. Peter, C. Y. Chen, R. Peter, A. A. Mitton and D. A. Klumpp, *Tetrahedron Lett.*, 2010, **51**, 4984–4987.
57 T. H. Pham, J. S. Olsson and P. Jannasch, *J. Mater. Chem. A*, 2019, **7**, 15895–15906.
58 W.-H. Lee, A. D. Mohanty and C. Bae, *ACS Macro Lett.*, 2015, **4**, 453–457.
59 J. S. Olsson, T. H. Pham and P. Jannasch, *J. Membr. Sci.*, 2019, **578**, 183–195.
60 D. R. Dekel, M. Amar, S. Willdorf, M. Kosa, S. Dhara and C. E. Diesendruck, *Chem. Mater.*, 2017, **29**, 4425–4431.
61 D. S. Pedersen and C. Rosenbohm, *Synthesis*, 2001, 2431–2434.